Journal of Catalysis **187,** 30–38 (1999)
Article ID jcat.1999.2614, available online at http://www.idealibrary.com on IDEAL®

A Sintering Study of Novel Sol–Gel-Based Nanocluster Catalysts[1]

Anthony Martino,*,[2] Allen G. Sault,† Jeffrey S. Kawola,* Elaine Boespflug,† and Mark L. F. Phillips‡

*Catalysis and Chemical Technologies Department, Sandia National Laboratories, Albuquerque, New Mexico 87185-0710; †New Materials Theory and Validation Department, Sandia National Laboratories, Albuquerque, New Mexico 87185-1349; and ‡Gemfire Corporation, 2440 Embarcadero Way, Palo Alto, California 94303

Received November 17, 1998; revised March 16, 1999; accepted June 28, 1999

We introduce two novel synthesis strategies to make nanoclusters on silica and alumina supports using inverse micelle technology and sol–gel processing. In the first method, sol–gel chemistry (hydrolysis and condensation of metal alkoxides) is performed in alcohol-free inverse micelle, metal cluster solutions. In the second method, metal clusters formed in traditional inverse micelle solutions are allowed to diffuse into preexisting wet monoliths formed using traditional sol–gel techniques. The different materials produced are characterized and compared with respect to particle size and the substrate properties using N_2 porosimetry methods, chemisorption, atomic absorption, and transmission electron microscopy. The effect of calcination on particle and support stability is determined and discussed in terms of the metal coverage and the relationship between particle size and pore dimensions. We conclude that the relative sizes of particles and pores has no clear effect on sintering behavior. Sintering appears to be predominately dependent on metal loading normalized against the support surface area suggesting Ostwald ripening as the sintering mechanism.

Key Words: **platinum; silica; alumina; clusters; sol–gel; sintering; inverse micelles.**

INTRODUCTION

Nanometer-sized metal clusters embedded in sol–gel-prepared metal oxide substrates form a unique class of catalytic materials. Sol–gel processing loosely defines the inorganic polymerization reactions of hydrolysis and condensation of metal alkoxides to form solid metal oxides (1). Because many synthesis parameters are available, sol–gel processing offers versatility in final material properties not available by other catalyst synthesis methods (2–5). For instance, by adjusting the oxide precursor type and concentration, the water to precursor reaction ratio, and whether the reactions are acid or base catalyzed, materials with controlled surface areas and pore dimensions are produced. Formation of metal oxide colloidal dispersions (sols) precedes final condensation into monolith, particulate, or thin film gels. Also, it is possible to tune molecular composition; SiO_2, Al_2O_3, TiO_2, and other pure species, as well as mixed metal oxides are formed. Atomic metals are added later to gels when salts are ion exchanged with terminal hydroxyl groups (6, 7), through impregnation of metal salts into the gel backbone (8–11) or through the use of chelating agents (12, 13). Reduced metal clusters are formed by chemical, thermal, and photolytic reduction. Again, the methods are versatile with respect to metal type, and Pt, Pd, and Ru are common.

In addition to versatility, metal cluster, sol–gel materials have specific catalytic advantages. For clusters synthesized by impregnation techniques and independent of metal type or support composition, some degree of occlusion of the particles within the metal oxide framework occurs (14–17). As a result, higher resistance to metal sintering is noticed. Also, sol–gel processing parameters have been used to control pore dimensions and particle sizes so that the particles are encapsulated (i.e., the pore size is approximately equal to the particle diameter) (18). Resistance to sintering increases without occlusion of the particles. In one case, however, lower activities were observed due to encapsulation (19). In another study, Pt/Al_2O_3 sol–gel-prepared materials showed resistance to coke formation for a number of different support and particle morphologies (20).

In this work, we introduce two novel synthesis strategies to make Pt particles embedded in sol–gel formulated SiO_2 and Al_2O_3, and we test sintering resistance. In an earlier study, we synthesized Au particles in SiO_2 by combining inverse micelle techniques with sol–gel processing in nonaqueous, alcohol-free surfactant solutions (21). We have now expanded the synthesis to include the formation of Pt particles and the formation of Al_2O_3 supports. We also develop a second synthesis approach in this paper; namely, inverse micelle-synthesized Pt clusters are encapsulated in *traditionally* synthesized sol–gel SiO_2 supports. The clusters

[1] This work is supported by the U.S. Department of Energy under Contract DE-AC04-94AL85000. Sandia is a multiprogram laboratory operated by Sandia Corporation, a Lockheed Martin Company, for the United States Department of Energy. The U.S. Government's right to retain a nonexclusive royalty-free license in and to the copyright covering this paper, for governmental purposes, is acknowledged.

[2] To whom correspondence should be addressed. E-mail: tmartino@vmresearch.org.

0021-9517/99 $30.00

are allowed to diffuse into the pores of a wet alcogel, and drying of the gel encapsulates the particles in the micropores. The synthesis methodologies we present offer the advantages of the inverse micelle technique to make clusters; namely, ultrasmall, monodispersed particles of controlled, tunable sizes are formed (22, 23). Also, the methodology offers a novel procedure to encapsulate particles in the support by building the metal oxide framework around the clusters. We study the sintering behavior of our samples.

We will soon report in a separate letter the activity, selectivity, and stability of our catalysts in the dehydrogenation of propane.

EXPERIMENTAL

Materials

The following materials were purchased from Aldrich Chemical Co. and were used as delivered: the surfactant didodecyldimethylammonium bromide (DDAB), tetraethylorthosilicate (TEOS), aluminum tri-*sec*-butoxide (97%), ethyl acetoacetate (99+%), platinum (II) chloride (98%), apolar solvent toluene (99.9+% purity), reducing agent lithium borohydride in tetrahydrofuran (2M), and a 40 wt% tetrabutylammonium hydroxide (TBAOH) in water solution. Acid and base solutions were made from HCl-certified 1 N solution and concentrated HNO_3 and NH_4OH certified ACS plus from Fisher Scientific. Absolute ethyl alcohol was obtained from AAPER alcohol.

Synthesis

The synthesis of nanoclusters via inverse micelle solutions is an established technique (22, 23). Metal salts are solubilized within the polar regions of inverse micelles. When a reducing agent is added, nucleation and growth of the metal particles commences. Stabilization of the growth is controlled by the surfactant, and final particle size depends on a number of synthesis variables. The synthesis of Au particles encapsulated in SiO_2 via an inverse micelle, sol–gel-combined procedure was described earlier (21, Fig. 1). Here, we extend the synthesis to include Pt particles and Al_2O_3 supports (Table 1).

Sequential inverse micelle, sol–gel-derived Pt/SiO_2. Surfactant is added to toluene (5 wt%) and stirred by hand shaking to form the inverse micelle solution. $PtCl_2$ (0.005 M) and the gel precursor TEOS (0.4 M) are added to the DDAB and toluene mixture, and the solution is stirred until the salt is fully solubilized. Sufficient $LiBH_4$/THF solution to result in a 3 : 1 ratio of $BH_4^- : Pt^{2+}$ is then injected into the salt precursor solution under rapid stirring to form the Pt clusters. The 40 wt% TBAOH in water solution is added to the mixture 5 min after the addition of the $LiBH_4$, and gelation is marked when the solution no longer flows

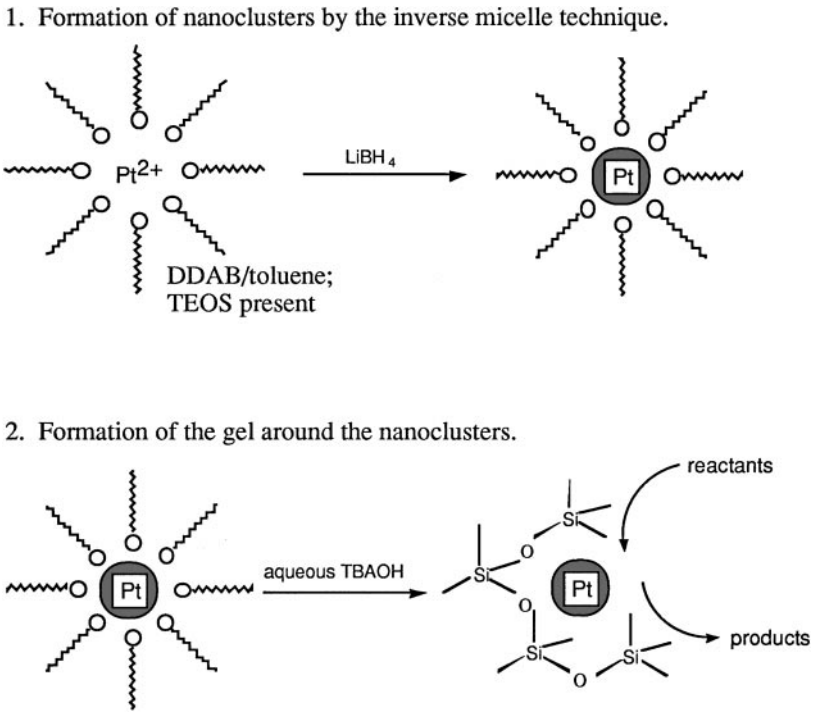

FIG. 1. Schematic representation of the "sequential" reaction method to form clusters embedded in gels. All reactants are initially present and the two reactions (metal salt reduction and sol-gel processing) are carried out in sequence. In the "concurrent" reaction methods, the two reactions are carried out separately and the two products (clusters in inverse micelles and wet monoliths) are mixed.

TABLE 1

Summary of Samples, Recipes, and Postsynthesis Treatments Used in this Study

Catalyst	Recipe	Postsynthesis treatment
Pt/SiO_2 xerogel	$Si \cdot 3H_2O \cdot 23$DDAB/Tol $\cdot$ 0.2 TBAOH $\cdot$ 0.005 M $PtCl_2$	Washed; 40, 50, 120°C air drying stages
Pt/SiO_2 aerogel	$Si \cdot 3H_2O \cdot 23$DDAB/Tol $\cdot$ 0.2 TBAOH $\cdot$ 0.005 M $PtCl_2$	Supercritical extraction: CO_2, 40°C
Pt/Al_2O_3 xerogel	$Al \cdot 3H_2O \cdot 14$DDAB/Tol $\cdot 0.2HNO_3 \cdot$ 0.005 M $PtCl_2$	Washed; 40, 50, 120°C air drying stages
Pt/Al_2O_3 aerogel	$Al \cdot 3H_2O \cdot 14$DDAB/Tol $\cdot 0.2HNO_3 \cdot$ 0.005 M $PtCl_2$	Supercritical extraction: CO_2, 40°C
Pt/SiO_2^* xerogel	$Si \cdot 4$EtOH $\cdot H_2O \cdot$ 0.007HCl; $0.1H_2O \cdot$ 0.05 M NH_4OH; 0.01 M $PtCl_2$	Washed; 40, 50, 120°C air drying stages

Note. The asterisk always refers to the sample synthesized by the "concurrent" procedure explained in the text.

under gravity. The water to gel precursor molar ratio is set at 3 : 1. The gels are aged for 2 days at 50°C and are washed with pure toluene (soaked for several hours at 50°C, three cycles) to remove any unattached surfactant, metal salt, or excess reducing agent. The samples are then split in two with half being used to form xerogels and the other half being used to form aerogels. Xerogels are formed by three staged drying cycles of 40, 50, and 120°C each overnight. Aerogels are formed under supercritical CO_2 extraction. The overall molar equivalent ratio of the synthesis is $Si : 3H_2O :$ 23 toluene : 0.2 TBAOH where the toluene value actually represents 0.005 M $PtCl_2$ in 5 wt% DDAB in toluene.

Sequential inverse micelle, sol–gel-derived Pt/Al_2O_3. The Pt/Al_2O_3 synthesis is loosely based on a previous alcohol based Al_2O_3 recipe without metal (19, 24). DDAB is added to toluene (5 wt%) and stirred by hand shaking to form the inverse micelle solution. The gel precursor is a 1 : 1 molar ratio of aluminum tri-*sec*-butoxide and ethyl acetoacetate. $PtCl_2$ (0.005 M) and the gel precursor (0.8 M) are added to the DDAB and toluene mixture, and the solution is stirred until the salt is fully solubilized. The $LiBH_4$/THF solution is then injected into the salt precursor solution to form the clusters under rapid stirring so that the $[BH_4^-] : [Pt^{2+}] = 3 : 1$. After 30 min, an aqueous 4.3 M HNO_3 solution is added and gelation is marked when the solution no longer flows under gravity. The water to gel precursor molar ratio is set at 3 : 1. The gels are aged for 2 days at 50°C and are washed with pure toluene (soaked for several hours at 50°C, three cycles) to remove any unattached surfactant, metal salt, or excess reducing agent. The samples are then split in two with half being used to form xerogels and the other half being used to form aerogels. Xerogels are formed by three staged drying cycles of 40, 50, and 120°C each overnight. Aerogels are formed under supercritical CO_2 extraction. The overall molar equivalent ratio of the synthesis is $Al : 3H_2O :$ 14 toluene : 0.2 HNO_3 where the toluene represents 0.005 M $PtCl_2$ in 5 wt% DDAB in toluene.

Concurrent inverse micelle, sol–gel-derived Pt/SiO_2^*. An asterisk denotes samples made by the "concurrent" methodology. Here, Pt clusters are synthesized with a "standardized" inverse micelle recipe. Concurrently, SiO_2 monolith is synthesized with a standardized ethanol sol–gel recipe. The clusters are then allowed to diffuse into the gel, and the gel is dried leading to encapsulation of the particles in the micropores. To form the clusters, 0.01 M $PtCl_2$ is solubilized in a 5 wt% DDAB, toluene mixture. The $LiBH_4$/THF solution is injected into the salt precursor solution under rapid stirring so that the $[BH_4^-] : [Pt^{2+}]$ ratio is 3 : 1. To form the SiO_2 monolith, a stock solution of 61 ml TEOS, 61 ml ethanol, 4.87 ml water, and 0.2 ml 1 M HCl is refluxed at 60°C for 1.5 h with stirring. The solution is stable indefinitely at 20°C, but is stored in a freezer to ensure stability. The approximate molar ratio of the solution is TEOS : 4 ethanol : H_2O : 0.007 HCl. Mixing a 10 : 1 volume ratio of stock solution to 0.5 M NH_4OH causes gelation within minutes. The gels are aged and washed three times with excess ethanol at 50°C for several hours. To produce the cluster/SiO_2 matrix, the gels are washed three times with excess toluene at 50°C for several hours. Then, the SiO_2 is washed with excess cluster solution three times at 50°C for several hours. Xerogels are formed by three staged drying cycles of 40, 50, and 120°C each overnight. The methodology was not extended to aerogels or Al_2O_3 supports, although this should be facile.

All samples were calcined in a tube furnace under air. A two-stage temperature ramp was used. The samples were held at 250°C for 1 h and then the final temperature for 1 h. Final calcine temperatures were determined by TGA results as discussed below.

Characterization

Metal weight fractions on the supports were determined with a Perkin–Elmer 5100PC atomic absorption spectrophotometer (AA). Thermogravimetric analysis (TGA) was completed with a TA Instruments Thermal Analyst 2000. Platinum particle size was characterized by transmission electron microscopy (TEM) with a 300-keV Phillips CM30 electron microscope. To prepare TEM samples, dried, crushed gels were dispersed over a holey carbon substrate. N_2 porosimetry, surface area analysis (BET) of the crushed xerogels and aerogels was carried out with a Quantachrome Autosorb-6 surface analysis apparatus. BET samples were outgassed for 20 h at 100°C. Pore size distributions were calculated with the Kelvin equation for the mesopores with the deBoer equation to correct for micropores. We present the desorption isotherm for the pore

size distribution calculations, as suggested by the Quantachrome manual. For practical purposes, our data shows no changes (<5–10% shift) in the pore distribution maxima for desorption vs adsorption isotherms (adsorption curves are generally broader). Hydrogen chemisorption was measured using a Coulter Omnisorp 100CX instrument. All chemisorption samples were calcined at 450°C in air for 1 h except the concurrently produced Pt/SiO_2^* sample. Based on TGA results, the concurrently produced Pt/SiO_2^* sample was calcined at 600°C for 1 h in air. In the chemisorption unit, the samples were outgassed in flowing He at 350°C for 1 h followed by reduction in flowing hydrogen at 400°C for 2 h. Samples were then evacuated at 405°C for 3 h prior to cooling to room temperature before measurement of hydrogen uptakes. Dispersions were calculated from total hydrogen uptake and converted to particle sizes by assuming spherical particles and a Pt atom surface density of 1.25×10^{15} atoms/cm^2. Three sets of samples were tested by AA to test the reproducibility of the synthesis on metal loadings. Only the first set of samples was used for TEM, chemisorption, and BET studies (i.e., those listed first and on the left in Table 3).

RESULTS

TGA weight loss results indicate a large difference between the samples produced by the sequential reactions of metal reduction, hydrolysis, and condensation and the Pt/SiO_2^* sample produced by the concurrent synthesis (Fig. 2). The weight loss is large on an absolute scale for the samples produced in the sequential methodology with greater than 50% weight loss. Most weight loss occurs below 400°C so 450°C was chosen as the calcination temperature. The Pt/SiO_2^* sample shows two weight loss regions, at approximately 350 and 550°C. Only 15 wt% of the total sample is lost. A temperature of 600°C was therefore chosen as the calcination temperature to ensure complete weight loss prior to analysis and testing. TGA results did not differ in air compared to an inert He atmosphere.

BET surface area results indicate a large difference between the samples produced by the sequential reactions and the SiO_2^* sample produced by the concurrent synthesis (Fig. 3). Sequentially produced Pt/SiO_2 and Pt/Al_2O_3 xerogels and aerogels are nonporous and show little surface area. Upon calcination surface area increases greatly. The same trend is observed with the Pt/SiO_2^* xerogel, but these samples are mesoporous with high surface areas even prior to calcining. Differential pore size analysis shows the Pt/SiO_2^* xerogel pores are larger with a broader pore size distribution then the other samples (Fig. 4). A representative adsorption and desorption isotherm is presented (Fig. 5).

Particle size was studied with TEM (Fig. 6) and H_2 chemisorption (Table 2). TEM analysis indicates the initial Pt/SiO_2 xerogel, Pt/SiO_2 aerogel, and the Pt/SiO_2^* xerogel particle diameters are 1.5, 1.5, and 2.0 nm, respectively. After calcination, TEM particle sizes increase to 4.5, 4.0, and 3.5 nm, respectively. The Al_2O_3 xerogel and aerogel show aggregated metal particles throughout the substrate. No individual particles are observed. After calcination, individual particles are observed. The Pt/Al_2O_3 xerogel and aerogel particle diameters are 3.5 and >50 nm, respectively. Particle sizes determined by chemisorption are compared to TEM results (Table 2). For the calcined Pt/SiO_2 and Pt/SiO_2^* aerogels and the calcined Pt/Al_2O_3 xerogel, the measured dispersions are 12.7, 22.3, and 11.1%, respectively, corresponding to particle diameters of 4.5, 2.5, and 4.9 nm, in close agreement with TEM results. H_2 chemisorption measurements were not possible on the uncalcined samples due to severe outgassing problems.

Atomic absorption spectroscopy was used to determine metal loadings. Three separate sample sets were tested

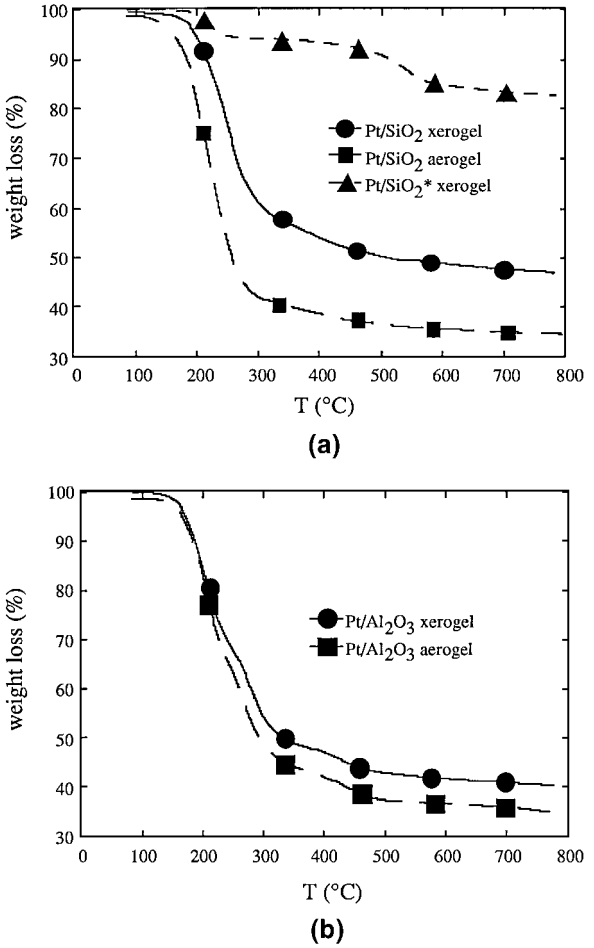

FIG. 2. TGA results to determine weight loss with temperature. In sequentially produced samples, over 50 wt% is lost due to unreacted gel precursor left by the inefficiency of sol-gel processing in inverse micelle solutions. The concurrently produced samples, using a well-studied synthesis procedure to produce silica monoliths, result in an efficient reaction and little loss. (a) SiO_2 samples. (b) Al_2O_3 samples.

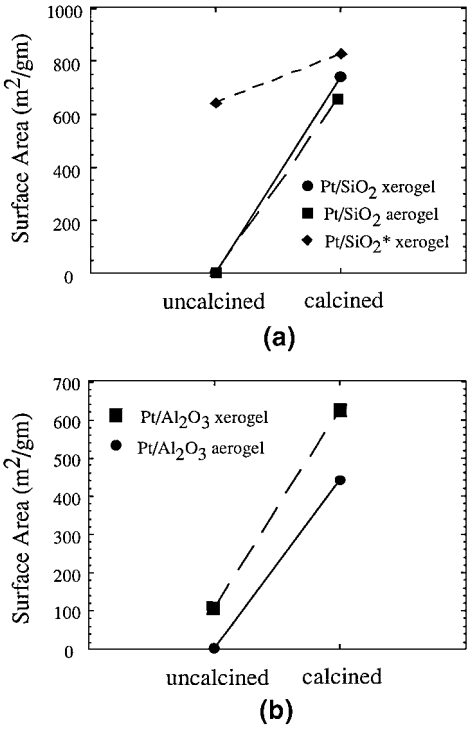

FIG. 3. N_2 porosimetry results to determine surface area in dried and calcined samples. In sequentially produced samples, removal of the unreacted TEOS upon calcination opens the pores and a large increase in surface area is observed. (a) SiO_2 samples. (b) Al_2O_3 samples.

(Table 3). The first set of numbers (on the left) represents the samples used for BET, TEM, and chemisorption. For the Pt/SiO_2 xerogel, Pt/SiO_2 aerogel, Pt/SiO_2^* xerogel, Pt/Al_2O_3 xerogel, and Pt/Al_2O_3 aerogel, the metal loadings are 0.24 ± 0.08, 0.23 ± 0.07, 0.25 ± 0.03, 0.22 ± 0.14, and 0.24 ± 0.14 wt%, respectively. Reproducibility is poor, but it is particularly poor with the Al_2O_3 samples indicating an extreme sensitivity of metal loading to synthesis conditions. It is possible to increase metal loadings by increasing precursor salt concentrations, but particle size and polydispersity generally increase.

DISCUSSION

Synthesis Effects on Support Properties

TGA results indicate that for samples synthesized via the sequential methodology (i.e., sol-gel processing is completed in an alcohol-free, cluster, inverse micelle system) over 50 wt% of the sample is thermally lost by about 400°C. The only single component present to such extent in the initial reaction mixture is the gel precursor TEOS leading us to believe that the large weight loss in the final product is due to unreacted TEOS monomer. It is likely that the unreacted TEOS results from inefficient hydrolysis and condensation reactions in apolar, alcohol-free inverse micelle mixtures. The same argument holds for the alumina system.

In samples synthesized via the concurrent methodology (i.e., using a well-defined sol-gel process taking place in ethanol followed by the addition of an already prepared cluster, inverse micelle solution), TGA results show

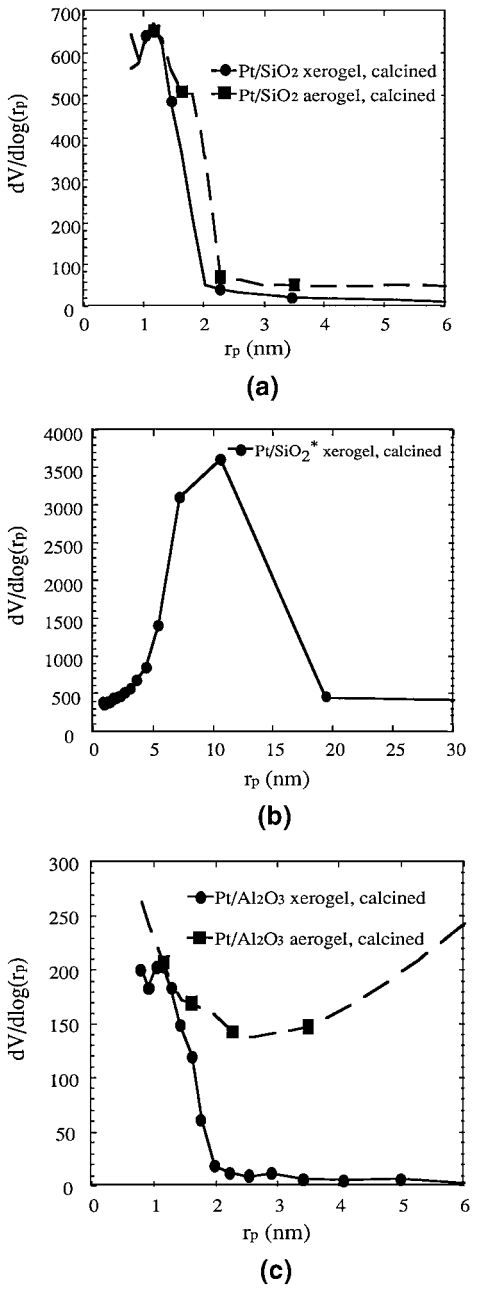

FIG. 4. Pore size distributions calculated from the porosimetry results. In sequentially produced samples, the pores are small and monodisperse falling on the limit of what is defined as mesoporous (pore sizes approximately 1 nm in diameter). There is little effect of calcination. In the concurrently synthesized sample, pore sizes are larger and more disperse. The average pore size is approximately 6 nm in diameter before calcination (not shown) and grows upon calcination to approximately 11 nm in diameter. (a) Sequentially produced SiO_2 samples; (b) concurrently produced SiO_2 sample; (c) sequentially produced Al_2O_3 samples. Only representative data points are shown. Lines represent the full data sets.

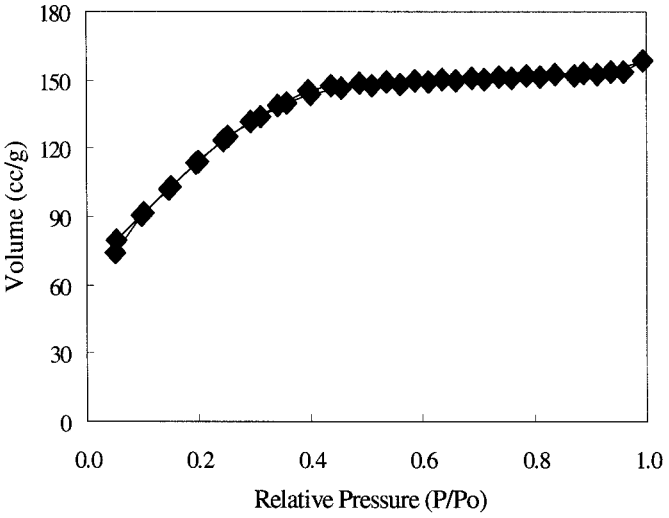

FIG. 5. A representative adsorption and desorption isotherm for monoliths produced in inverse micelle solutions. Isotherm shown is for calcined Pt/SiO_2 xerogel.

two weight loss regions with a total loss of approximately 12 wt%. No weight loss occurs before 200°C indicating that all solvents were removed in the drying procedure. At approximately 200°C, there is a loss of about 6 wt% mostly due to the thermal breakdown of surfactant. There is little unreacted TEOS due to the highly studied, efficient synthesis procedure used. Finally, starting at approximately 400°C, about 5 wt% is lost probably due to the thermal breakdown of terminal hydroxy groups.

The N_2 porosimetry results support our TGA analysis. In sequentially synthesized samples, no measurable surface area exists before calcination, because of the presence of surfactant and unreacted TEOS in the pores. The surface area increases greatly upon thermal removal of these components. In the concurrently synthesized sample, surface area increases slightly due to removal of surfactant.

In our earlier work, we studied the synthesis parameters that govern final material properties in sol–gel-processed materials in inverse micelle systems (21). We observed, as we observe here, that monoliths form at much lower water: TEOS ratios than in alcohol-based systems. We speculate that monoliths form due to localized high water concentration regions in the inverse micelles with the hydrolysis and condensation reaction mechanisms taking place across surfactant monolayers and in transient micelle material exchange states. It appears in these mechanisms that only a fraction of TEOS is exposed to the water-rich regions and participates in the reaction, thus providing a high effective water concentration as we speculated earlier. Also in our previous work, we noticed a reverse trend in surface area with the water: TEOS ratio than is typically found in alcohol systems. As the samples in our previous study were not calcined, it is unfortunate that we were measuring surface areas of materials obstructed with unreacted TEOS. True monolithic surfaces were not measured calling into question the analysis of the effect of the water: TEOS ratio in that work.

TABLE 2

Summary of Particle Diameters as Determined by TEM

	Particle diameter (nm)		
		Postcalcination	
Catalyst	Postsynthesis TEM	TEM	Chemisorption
Pt/SiO_2 xerogel	1.5	4.5	4.5
Pt/SiO_2 aerogel	1.5	4.0	
Pt/Al_2O_3 xerogel	Aggregated	3.5	4.9
Pt/Al_2O_3 aerogel	Aggregated	>50	
Pt/SiO_2^* xerogel	2.0	3.5	2.5

Note. TEM results are compared to chemisorption results for the postcalcined samples.

TABLE 3

Summary of Weight Percent Metal Loading as Determined by Atomic Absorption (AA)

	Metal loading (wt%)	
Catalyst	Uncalcined	Calcined
Pt/SiO_2 xerogel	0.16, 0.25, 0.31	0.32, 0.50, 0.62
Pt/SiO_2 aerogel	0.15, 0.27, 0.26	0.43, 0.77, 0.74
Pt/Al_2O_3 xerogel	0.20, 0.10, 0.37	0.50, 0.25, 0.92
Pt/Al_2O_3 aerogel	0.37, 0.10, 0.26	1.06, 0.29, 0.74
Pt/SiO_2^* xerogel	0.25	0.30

Note. Measurements on multiple samples show the reproducibility of the synthesis. Only the samples whose metal loadings are represented in the left-most column are used in BET, TEM, chemisoption, and catalyst testing experiments.

Synthesis Effects on Particle Properties

TEM results indicate that the metal reduction reaction to form clusters is highly efficient in the SiO_2 samples. Small, monodisperse particles with diameters of less than 2 nm are typical for Pt particles synthesized in pure DDAB/toluene inverse micelle mixtures. Visually, an abrupt color change and rapid H_2 gas production indicate an instantaneous reaction. In the sequential reduction methodology, the presence of TEOS, the hydrolysis and condensation reactions, and drying have no effect on final particle size (2-nm diameter Pt particles are synthesized in pure DDAB/toluene solutions). In the concurrent reduction methodology, diffusion of the particles into the gel network and drying have no effect on final particle size.

The reduction reaction efficiency decreases substantially in alumina systems. Visually, color change and H_2 production occur over at least 0.5 h. In reactions in inverse micelles,

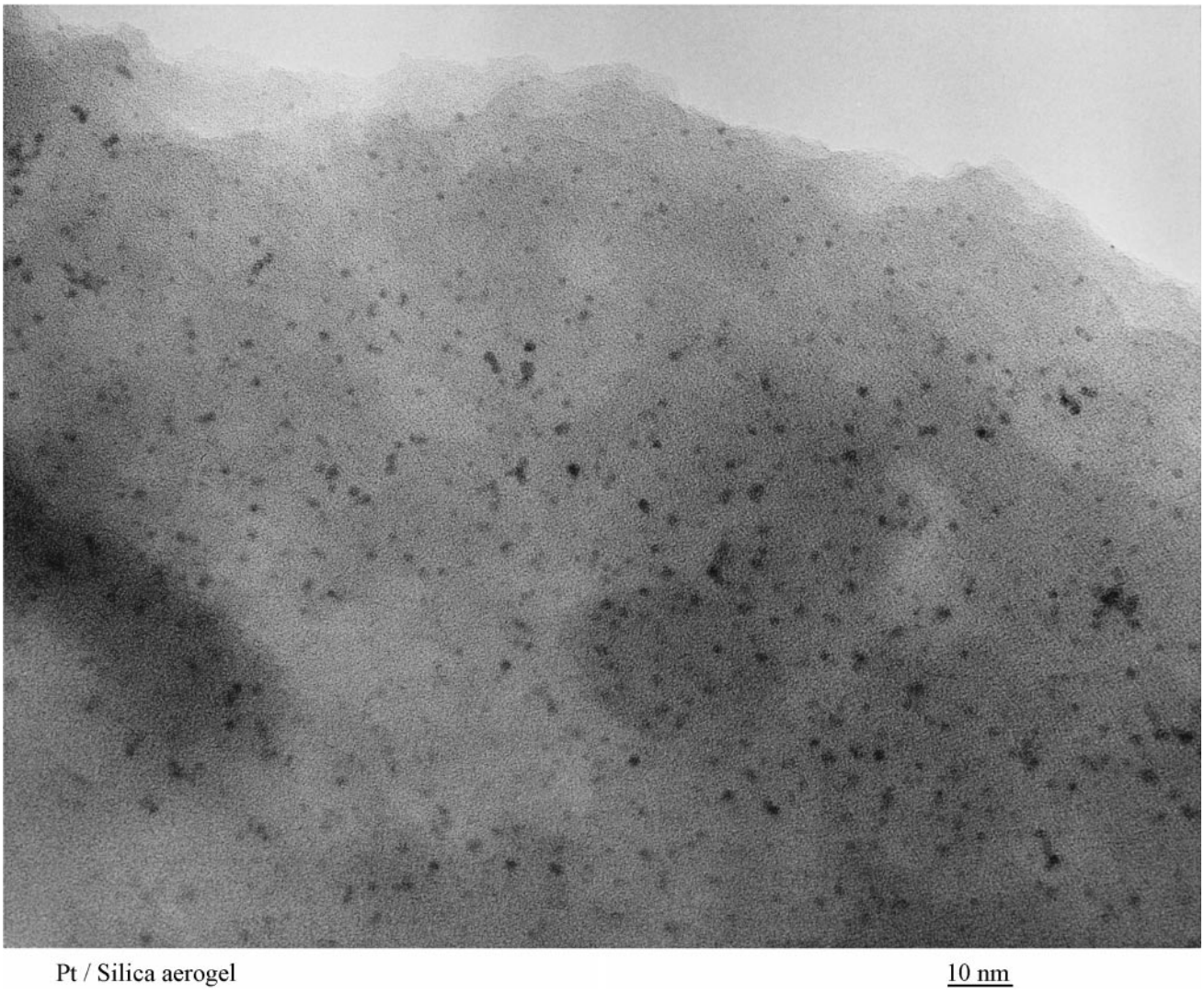

FIG. 6. Representative TEM picture of inverse micelle cluster, sol-gel-derived materials. Sample shown is of Pt clusters on a SiO_2 aerogel support before calcination.

it is known that slow nucleation and growth results in large, polydisperse size distributions. We observe similar results here. Particularly poor reproducibility in metal loadings also indicates inefficiency in the metal reduction reaction. Further, the particles are aggregated indicating surfactant stabilization was not effective. A concurrent reaction mechanism where the particles are synthesized separately maybe required to obtain highly dispersed Pt particles in aluminum gels. We have not yet studied a concurrent reaction mechanism for alumina.

The Dominant Mechanism of Sintering

In the sequentially synthesized SiO_2 samples, particles are most likely occluded in unreacted TEOS prior to calcination. After calcination, the particle size increases to approximately three times larger than the pore dimensions even at the relatively low calcination temperatures of 450°C. Agreement between TEM and chemisorption results indicates that the particles are moving out of the pores and onto the surface of the substrates rather than being occluded in the support structure.

In the concurrently synthesized Pt/SiO_2^* xerogel, particle size is approximately three times smaller than the pore dimension before calcination. After calcination, the particle size and the pore dimensions grow only slightly (i.e., no sintering), the particle size remains approximately three times smaller than the pore dimension. Agreement between TEM and chemisorption results indicates no particle occlusion.

It is clear from the above results that no clear relationship between particle size and pore dimension affects sintering behavior. Previous work on Pt/SiO_2 catalysts (18) states that there is a strong relationship between particle size and pore size and that for low metal loadings sintering is prevented

when particle sizes match average pore diameters. The conclusions of this previous work were based upon three distinct cases: (i) "high" (>0.5 wt%) Pt loadings with particle sizes smaller than the pore size; (ii) "high" Pt loadings with particle sizes matched to the pore size; and (iii) "low" (<0.3 wt%) Pt loadings with particle sizes matched to the pore size. The fourth case, low Pt loadings with particle sizes smaller than the pore size, was not studied. Thus, the possibility that sintering resistance is merely a reflection of only Pt loading could not be eliminated. The concurrently synthesized Pt/SiO_2^* xerogel reported here falls into the fourth case and demonstrates resistance to sintering even though the particle size and pore size are not well matched. Our results for the Pt/SiO_2^* sample when compared to previous work are further evidence that there is no clear relationship between particle size and pore dimension affecting sintering behavior.

The combined results of the previous work (18) with the results presented here provide strong evidence that sintering is a function of metal coverage. If metal coverage is defined as the metal loading normalized against the surface area of the support (g Pt/m^2 of support), and we plot the factor increase in metal particle size (i.e., amount of sintering) as a function of metal coverage (Fig. 7), we see a definite correlation. The degree of sintering increases with Pt coverage. It is important to reiterate that the sintering is not observed as a function of metal loading. Within our study, the Pt/SiO_2 xerogel and the Pt/SiO_2^* xerogel have similar metal loadings, but different sintering behavior is observed. *Metal coverage* as defined above is the dominant effect.

Metal particle sintering on support materials occurs by two mechanisms: (1) particle aggregation due to particle diffusion along the support, and (2) Ostwald ripening where large particles grow at the expense of smaller particles due to atomization and diffusion between particles. As both mechanisms are dependent on particle concentration (i.e., number of particles per unit area) and metal coverage is closely related to concentration, both particle diffusion and Ostwald ripening would be expected to display the behavior shown in Fig. 7. If, however, we accept that particle migration is hindered in cases where the pore size and particle size match, we can conclude that Ostwald ripening is the predominate sintering mechanism. To see this, consider the behavior of the Pt/SiO_2^* sample relative to the 0.2 wt% Pt/SiO_2 sample of Zou and Gonzales (18). Both samples have similar metal loadings, Pt particle sizes, and surface areas, but differ substantially in terms of pore size distribution; the sample of Zou and Gonzales shows a good match between pore size and particle size, while the pores in the Pt/SiO_2^* sample are much larger than the particle size. As a result, particle diffusion should be much faster in the Pt/SiO_2^* sample, yet both samples exhibit similar sintering behavior. We therefore conclude that particle diffusion is not the dominant sintering mechanism under the conditions tested. Thus, while matching particle size and pore size may have an inhibiting effect on particle diffusion, we conclude that Ostwald ripening is not inhibited by such matching. It may be possible to effect vapor pressures and influence surface tensions by encapsulation such that the mechanism for Ostwald ripening is hindered, but there is yet no experimental evidence to quantify the effects.

The effect of calcination on particle size in alumina samples is counterintuitive. Encapsulation is not an issue, because the particles and aggregates are much larger than the pore dimensions. With calcination, aggregated particles separate into smaller domains. In alumina samples, random particle diffusion upon calcination apparently decreases the particle concentration gradient resulting in more dispersed, smaller particles.

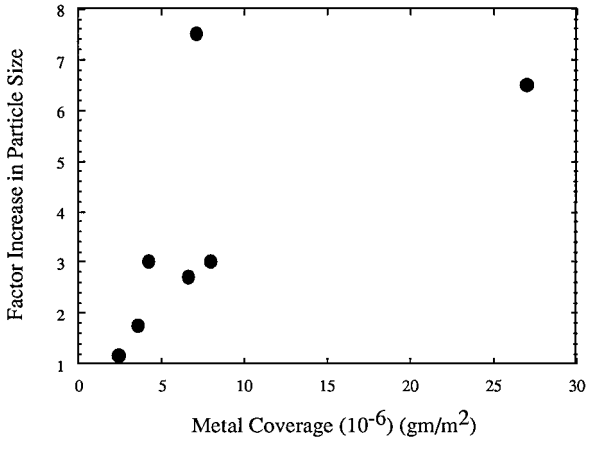

FIG. 7. The factor increase of particle size (i.e., degree of sintering) as a function of metal coverage shows a correlation. Metal coverage is defined as the weight of platinum in a sample divided by the surface area of the support. The degree of sintering increases with metal coverage indicating that the dominant mechanism of sintering is concentration-dependent Ostwald ripening. The data presented are taken from this work and previous work (18).

CONCLUSIONS

We introduce two novel synthesis strategies to make nanoclusters on silica and alumina supports using inverse micelle technology and sol-gel processing. In the first methodology, sol–gel chemistry is performed in alcohol-free inverse micelle, metal cluster solutions. Hydrolysis and condensation reactions are inefficient, but nonetheless monoliths form around the clusters. In the second method, metal clusters formed in traditional inverse micelle solutions are allowed to diffuse into preexisting monoliths formed using traditional sol–gel techniques (hydrolysis and condensation in ethanol). The two techniques give materials with similar cluster sizes, but different pore dimensions. We conclude that the relative sizes of particles and pores has no clear effect on sintering behavior. Sintering appears to be predominately dependent on metal coverage, defined as the

metal loading normalized against the support surface area, suggesting Ostwald ripening as the sintering mechanism.

REFERENCES

1. Brinker, C. J., and Scherer, G. W., "Sol-Gel Science." Academic Press, San Diego, 1990.
2. Ward, D. A., and Ko, E. I., *I&EC Res.* **34**, 421 (1995).
3. Schneider, M., and Baiker, A., *Catal. Rev.-Sci. Eng.* **37**, 515 (1995).
4. Cauqui, M. A., and Rodriquez-Izquierdo, J. M., *J. Non-Cryst. Solids* **147 & 148**, 724 (1992).
5. Pajonk, G. M., *Appl. Catal.* **72**, 217 (1991).
6. Tominaga, H., Ono, Y., and Keii, T., *J. Catal.* **40**, 197 (1975).
7. Ikoma, S., Takano, S., Nomoto, E., and Yokoi, H., *J. Non-Cryst. Solids* **113**, 130 (1989).
8. Morke, W., Lamber, R., Schubert, U., and Breitscheidel, B., *Chem. Mater.* **6**, 1659 (1994).
9. Ishiyama, J. I., Kurokawa, Y., Nakayama, T., and Imaizumi, S., *Appl. Catal.* **40**, 139 (1988).
10. Lopez, T., Villa, M., and Gomez, R., *J. Phys. Chem.* **95**, 1690 (1991).
11. Lopez, T., Lopez-Gaona, A., and Gomez, R., *Langmuir* **6**, 1343 (1990).
12. Moon Choi, K., and Shea, K. J., *J. Am. Chem. Soc.* **116**, 9052 (1994).
13. Hardee, J. R., Tunney, S. E., Frye, J., and Stille, J. K., *J. Polym. Sci., A: Polym. Chem.* **28**, 3669 (1990).
14. Azomoza, M., Lopez, T., Gomez, R., and Gonzalez, R. D., *Catal. Today* **15**, 547 (1992).
15. Lopez, T., Herrera, L., Gomez, R., Zou, W., Robinson, K., and Gonzalez, R. D., *J. Catal.* **136**, 621 (1992).
16. Gomez, R., Lopez, T., Castillo, S., and Gonzalez, R. D., *J. Sol-Gel Sci. Technol.* **1**, 205 (1994).
17. Lopez, T., Bosch, P., Navarrete, J., Azomoza, M., and Gomez, R., *J. Sol-Gel Sci. Technol.* **1**, 193 (1994).
18. Zou, W., and Gonzalez, R. D., *Appl. Catal. A* **102**, 181 (1993).
19. Mizushima, Y., and Hori, M., *Appl. Catal. A* **88**, 137 (1992).
20. Balakrishnan, K., and Gonzalez, R. D., *J. Catal.* **144**, 395 (1993).
21. Martino, A., Yamanaka, S. A., Kawola, J. S., and Loy D. A., *Chem. Mater.* **9**, 423 (1997).
22. Bradley, J. S., "Clusters and Colloids: From Theory to Applications" (G. Schmid, Ed.), Chapter 6. VCH, 1994.
23. Steigerwald, M. L., and Brus, L. E., *Annu. Rev. Mater. Sci.* **19**, 471 (1989).
24. Bonhomme-Coury, L., Babonneau, F., and Livage, J., *J. Sol-Gel Sci. Technol.* **3**, 157 (1994).